properties and meteorological conditions. *Int. J. Remote Sensing*, 2011, **32**(14), 3967–3984.
10. Gill, J. P. S., Yackel, J. J., Gekdsetzer, T. and Fuller, C., Sensitivity of C-band synthetic aperture radar polarimetric parameters to snow thickness over landfast smooth first year sdea ice. *Remote Sensing Environ.*, 2015, **166**, 34–49.
11. Vogelzang, J. and Stoffelen, A., Scatterometer wind vector products for application in meteorology and oceanography. *J. Sea Res.*, 2012, **74**, 16–25.
12. Bothale, Rajashree, Anoop, S., Rao, V. V., Dadhwal, V. K. and Krishnamurthy, Y. V. N., Understanding relationship between melt/freeze conditions derived from spaceborne scatterometer and field observations at Larsemann hills, East Antarctica during austral summer 2015–16. *Curr. Sci.*, 2017, **113**(4), 733–742.
13. Dugan, H. A., Arcone, S. A., Obryk, M. K. and Doran, P. T., High-resolution ground-penetrating radar profiles of perennial lake ice in the McMurdo Dry Valleys, Antarctica: Horizon attributes, unconformities, and subbottom penetration. *Geophysics*, **81**(1), WA13-WA20.
14. https://www.esrl.noaa.gov/psd/data/gridded/
15. https://www.esrl.noaa.gov/psd/data/gridded/tables/sst.html
16. Reynolds, R. W., Smith, T. M., Liu, C., Chelton, D.B., Casey, K. S. and Schlax, M. G., Daily high resolution blended analyses for sea surface temperature. *J. Climate*, **20**, 5473–5496.
17. Tedesco, M., *Remote Sensing of the Cryosphere* (ed. Tedesco, M.), Library of Congress Cataloging-in-Publication Data, Wiley Blackwell, 2015.
18. Adodo, F. I., Remy, F. and Picard, G., Seasonal variations of the backscattering coefficient measured by radar altimeters over the Antarctic Ice Sheet. *Cryosphere*, 2018, **12**, 1767–1778.
19. Markus, T. and Cavalieri, D. J., Interannual and regional variability of Southern Ocean snow on sea ice. *Ann. Glaciol.*, 2006, **44**, 53–57.
20. Dumas, J. A., Flato, G. M. and Brown, R. D., Future projections of land fast ice thickness and duration in the Canadian Arctic. *J. Climate*, 2006, **19**(20), 5175–5189.

ACKNOWLEDGEMENTS. We acknowledge the Indian Space Research Organisation for granting permission to participate in 35th ISEA. We are grateful to the National Centre for Antarctic and Ocean Research (NCAOR), Ministry of Earth Sciences for making all the expedition arrangements and would like to thank IIG, Mumbai for AWS data. The snow and ice depth data received from Russian station Progress II is gratefully acknowledged. The support received from Shri Raghvendra, Leader, Bharati station and all the members of 35th ISEA, Dr Ajay Dhar, IIG, Mumbai, Dr Shrivastava, GSI during ground truth acquisition is also thankfully acknowledged.

Received 15 February 2018; revised accepted 23 April 2018

doi: 10.18520/cs/v115/i3/552-559

A damage constitutive model for the intermittent cracked rock mass under the planar complicated stress condition

Hongyan Liu* and Fengjin Zhu

College of Engineering and Technology,
China University of Geosciences (Beijing), Beijing 100083, P.R. China

The calculation of rock mass damage induced by the intermittent crack is the premise for establishment of the rock mass damage constitutive model (DCM). However, there are two shortcomings in the previous calculation methods of the rock mass damage: (a) it only considers the crack geometry or strength parameters, and does not consider its deformation parameter such as normal and shear stiffness; and (b) the influence of loading condition of the rock mass is not considered. This study focuses on intermittent cracked rock mass under the planar complicated stress condition and calculates its damage tensor. The proposed calculation method of rock mass damage considers the crack parameter such as length, dip angle, internal friction angle, normal and shear stiffness (internal factor) as well as the loading condition (external factor). The corresponding DCM for the intermittent cracked rock mass is then set up. The calculation examples validate that the proposed model can reflect the influence of crack parameter and loading condition on the rock mass mechanical behaviour.

Keywords: Damage, intermittent cracked rock mass, planar complicated stress condition, stress intensity factor, strain energy density criterion.

THE mechanical behaviour of rock mass such as its strength and deformability under the complicated stress condition is one of the most important issues in practical engineering. Cracks affect the rock mass mechanical behaviour and failure mode to a large extent[1–6]. Wang and Huang[1,2] set up a constitutive model for the rock mass to reflect its strength and deformation anisotropy caused by the persistent joint. Tokiwa *et al.*[3] found that the rock mass deformability was controlled by the fault system in a shaft excavation in soft rock. Sari[4] assumed that the rock mass mechanical property was affected by the discontinuity characteristic and intact rock property. Through experimental and numerical analysis, Sagong *et al.*[5] found that the joint dip angle had much effect on the rock fracture and joint sliding behaviours around an opening in a jointed rock mass. Khani *et al.*[6] found that the rock mass deformational modulus and Poisson's ratio greatly decreased with the increase in fracture intensity. As the cracks are often many and intermittent, their influence on rock mass mechanical property cannot be

*For correspondence. (e-mail: lhy1204@cugb.edu.cn)

considered one by one. Studies were carried out with damage mechanics. The crack is assumed to be a kind of damage to the rock mass, which can be described with the damage[7,8]. However adopting a suitable damage tensor to describe the damage induced by cracks is the key to establishing the rock mass DCM. The definition of rock mass damage tensor induced by cracks often falls into two categories. One is to define the damage tensor in the rock mass geometry damage theory[7]. It only considers the crack geometry parameter such as its length and dip angle, while the crack strength such as its internal friction angle and cohesion is not considered. Li *et al.*[8] therefore set up a new damage tensor calculation method based on the energy principle of damage and fracture mechanics. We call it the geometry and strength damage tensor calculation method. It can consider the influence of crack geometry parameter and strength one on the rock mass damage. Compared to the former, the latter is better although not perfect. Three kinds of crack parameter such as its geometry one, strength one and deformation one like the crack normal and shear stiffness are proposed to describe the physical and mechanical properties. Meanwhile some studies show that the crack deformation parameter also has some influence on rock mass mechanical property. For example, it was found[9] that an increase in crack normal and shear stiffness would reduce the tensile stress at crack tips and then increase the rock mass strength. However, both the calculation methods for the damage tensor described do not consider the influence of crack deformation parameter.

Meanwhile this is still an important subject as the rock mass damage is related not only to the rock mass physical and mechanical property (internal factor) but also to the loading condition (external factor). For example, the rock mass biaxial and triaxial compressive strength is much larger than its uniaxial one. In other words, the rock mass damage under biaxial and triaxial compression is much lower than that under uniaxial compression. A new rock mass DCM is therefore established which can consider the co-influence of rock mass and the loading condition on the rock mass mechanical behaviour. Some examples are illustrated to validate this.

Yang *et al.*[10] ran the conventional triaxial compression test on the intact coarse crystal marble samples and intermittent cracked ones under different confining pressures. The samples are cylinders (50 mm in diameter and 100 mm in length), and the cracked ones have two unilateral and intermittent cracks with the depth of 0.3–0.5 mm filled with plaster shown in Figure 1. In order to study the influence of confining pressure on the cracked rock mass strength, compression tests were done. The compressive strength of samples with the confining pressure 0, 10, 20 and 30 MPa is 17.2, 90.4, 122.3 and 154.5 MPa respectively, and its failure modes are shown in Figure 1. Xie[11] assumed that damage progressively reduced rock mass cohesion and the volume element failure was caused by microcracks in it under loading. That is to say, the damage can be defined by deterioration of rock mass strength. Many researchers[12,13] also adopted this method to define rock mass damage. The damage of rock mass under different confining pressures can be calculated (Table 1). It indicates that rock mass damage decreases with increasing confining pressure, which shows that external factors (the load) affect the rock mass damage even if the internal factors (the rock mass sample and the crack) are identical. Therefore, the influence of loading condition on rock mass damage should be considered at the same time and only then the rock mass mechanical behaviour can be reflected properly.

For a planar problem in fracture mechanics, the increment of additional strain energy U_1 induced by the cracks is[8]

$$U_1 = \int_0^A G \, \mathrm{d}A = \frac{1}{E'} \int_0^A (K_\mathrm{I}^2 + K_\mathrm{II}^2) \, \mathrm{d}A, \tag{1}$$

where A is the crack area, G the energy release rate, and K_I and K_II are first and second stress intensity factors at the crack tip respectively. For a planar stress and strain problem, $E' = E$ and $E' = E/(1 - \nu^2)$ are adopted respectively, where E and ν are Young's elastic modulus and Poisson's ratio of the corresponding intact rock respectively. Here $E' = E$ is adopted because the planar stress problem is studied.

For one crack, $A = Ba$ (unilateral crack) or $2Ba$ (central crack). For many cracks, $A = NBa$ (unilateral crack) or $2NBa$ (central crack), where N is the crack number, B the crack depth and a the crack half length, as shown in Figure 2.

For the rock mass with one intermittent crack (shown in Figure 2) under the planar complicated stress, its damage strain energy Y is[14]

$$Y = -\frac{\sigma_\mathrm{eq}^2}{2E(1-D)^2} \left\{ \frac{2}{3}(1+\nu) + 3(1-2\nu) \left(\frac{\sigma_m}{\sigma_\mathrm{eq}} \right)^2 \right\}, \tag{2}$$

where, $\sigma_m = 1/3(\sigma_x + \sigma_y)$ is the hydrostatic stress,

$$\sigma_\mathrm{eq} = \frac{1}{\sqrt{2}} \sqrt{\sigma_x^2 + (\sigma_x - \sigma_y)^2 + \sigma_y^2 + 6\tau_{xy}^2}$$

is Mises effective stress, D the rock mass damage induced by the intermittent crack, and σ_x, σ_y and τ_{xy} are the normal stresses along x-axial and y-axial, the shear stress respectively.

Assume U^E is the unit volume elastic strain energy of the sample. Under the planar stress, it is[14]

$$U^E = -(1-D)Y. \tag{3}$$

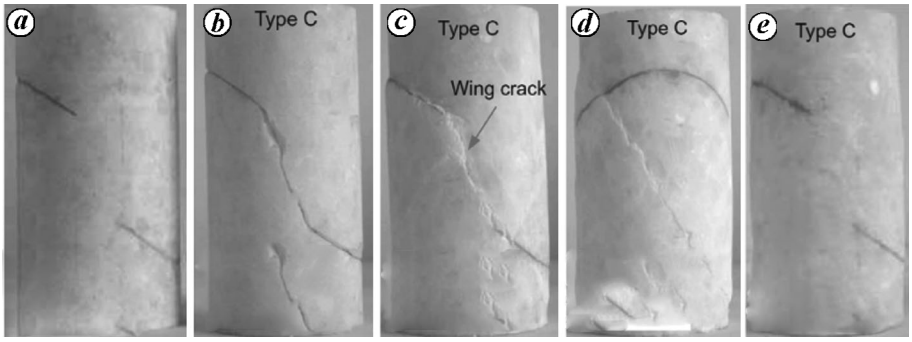

Figure 1. The sample with intermittent cracks of 45°dip angle and its failure modes under different confining pressure σ_3: ***a***, the cracked sample; ***b***, σ_3 = 0 MPa; ***c***, σ_3 = 10 MPa; ***d***, σ_3 = 20 MPa; ***e***, σ_3 = 30 MPa.

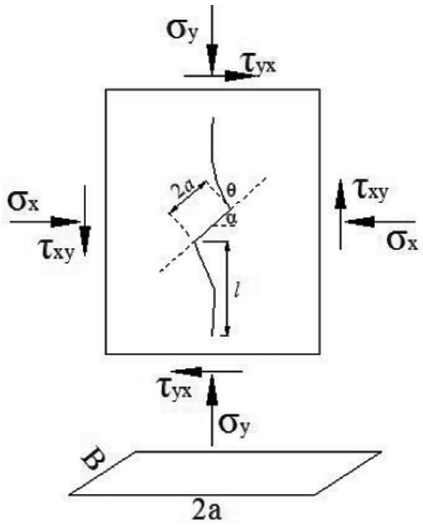

Figure 2. The wing crack growth model under the planar complicated stress. Crack length 2*a*, crack dip angle α, wing crack length *l*, crack depth *B*.

Table 1. Compressive strength of intact and cracked marble under different confining pressures

	σ_3 = 0 MPa	σ_3 = 10 MPa	σ_3 = 20 MPa	σ_3 = 30 MPa
σ_{imax}/MPa	71.39	102.0	108.06	128.44
σ_{cmax}/MPa	16.43	80.92	102.0	123.42
Damage	0.77	0.21	0.056	0.039

Damage = 1 – $\sigma_{cmax}/\sigma_{imax}$, where σ_{imax} and σ_{cmax} are the peak strength of intact and cracked rock mass.

Combining eqs (2) and (3) yields

$$U^E = -\frac{\sigma_{eq}^2}{2E(1-D)}\left\{\frac{2}{3}(1+\nu)+3(1-2\nu)\left(\frac{\sigma_m}{\sigma_{eq}}\right)^2\right\}. \quad (4)$$

When the rock mass has no cracks, $D = 0$, and eq. (4) can be written as

$$U_0^E = -\frac{\sigma_{eq}^2}{2E}\left\{\frac{2}{3}(1+\nu)+3(1-2\nu)\left(\frac{\sigma_m}{\sigma_{eq}}\right)^2\right\}. \quad (5)$$

The elastic strain energy increment of the rock mass per volume induced by the crack is

$$\Delta U^E = U^E - U_0^E = \left(\frac{\sigma_{eq}^2}{2E(1-D)} - \frac{\sigma_{eq}^2}{2E}\right) \times \left\{\frac{2}{3}(1+\nu)+3(1-2\nu)\left(\frac{\sigma_m}{\sigma_{eq}}\right)^2\right\}. \quad (6)$$

Assume the rock mass volume is V, the elastic strain energy increment induced by the crack is

$$\Delta U^E = V\left(\frac{\sigma_{eq}^2}{2E(1-D)} - \frac{\sigma_{eq}^2}{2E}\right) \times \left\{\frac{2}{3}(1+\nu)+3(1-2\nu)\left(\frac{\sigma_m}{\sigma_{eq}}\right)^2\right\}. \quad (7)$$

ΔU^E in eq. (7) and U_1 in eq. (1) are both the elastic strain energy increment induced by the crack, therefore they should be identical to each other

$$\Delta U^E = U_1, \quad (8)$$

or

$$\frac{1}{E}\int_0^A (K_I^2 + K_{II}^2)\mathrm{d}A = V\left(\frac{\sigma_{eq}^2}{2E(1-D)} - \frac{\sigma_{eq}^2}{2E}\right) \times \left\{\frac{2}{3}(1+\nu)+3(1-2\nu)\left(\frac{\sigma_m}{\sigma_{eq}}\right)^2\right\}. \quad (9)$$

From eq. (9) yields

$$D = 1 - 1/\left[1 + \frac{2}{V} \frac{1}{\sigma_{\text{eq}}^2 \left\{ \frac{2}{3}(1+\nu) + 3(1-2\nu)\left(\frac{\sigma_m}{\sigma_{\text{eq}}} \right)^2 \right\}} \times \int_0^A (K_{\text{I}}^2 + K_{\text{II}}^2) \mathrm{d}A. \right] \quad (10)$$

The solution of K_{I} and K_{II} is illustrated below.

Under the planar complicated stress condition, the crack will close and the normal and shear stresses will occur on the crack face. The shear stress will make the rock mass slide along the crack face and on the contrary the friction stress produced by the normal stress will resist this slide. With continued loading, the rock mass will slide along the crack face when shear stress exceeds friction stress. Accordingly, wing crack will occur at the crack tips and then begin to propagate[15,16] (Figure 2).

For the intact rock, under the planar complicated stress condition, the normal and shear stresses on the oblique plane with dip angle α are

$$\begin{cases} \sigma'_\alpha = \dfrac{\sigma_x + \sigma_y}{2} + \dfrac{\sigma_y - \sigma_x}{2} \cos 2\alpha - \tau_{xy} \sin 2\alpha \\ \tau'_\alpha = \dfrac{\sigma_y - \sigma_x}{2} \sin 2\alpha + \tau_{xy} \cos 2\alpha, \end{cases} \quad (11)$$

where σ'_α and τ'_α are the normal and shear stresses on the oblique plane respectively, and α is the oblique plane dip angle.

However, for the cracked rock mass, when an intermittent crack with length $2a$ exists on the oblique plane with dip angle α, the normal and shear stresses on this plane will be affected by the crack mechanical property which is less than that of the intact rock. So the normal and shear stresses on the crack face are

$$\begin{cases} \sigma_\alpha = (1 - C_n)\sigma'_\alpha \\ \tau_\alpha = (1 - C_t)\tau'_\alpha, \end{cases} \quad (12)$$

where C_n and C_t are the crack transferring compression and shear coefficients respectively[17]

$$C_n = \frac{\pi a}{\pi a + \dfrac{E}{(1-\nu^2)K_n}}, \qquad C_t = \frac{\pi a}{\pi a + \dfrac{E}{(1-\nu^2)K_s}}.$$

When the crack half-length $a = 0$ cm, namely the rock mass is intact, $C_n = C_t = 0$. Then eq. (12) is the same as eq. (11).

If we assume that crack cohesion and internal friction angle are c and φ respectively, the friction coefficient of the crack face is $\mu = \tan\varphi$. Then under the complicated stress condition, the slide force τ_{eff} along the crack face can be obtained by combining eqs (11)–(12)

$$\tau_{\text{eff}} = \begin{cases} 0 & \tau_{\text{eff}} \le 0 \\ \tau_\alpha - \mu\sigma_\alpha - c & \tau_{\text{eff}} > 0. \end{cases} \quad (13)$$

K_{I} and K_{II} at the crack tips can be calculated according to Lee *et al.*[18]

$$\begin{cases} K_{\text{I}} = \dfrac{2a\tau_{\text{eff}} \cos\alpha}{\sqrt{\pi(l + l^*)}} - \sigma_x \sqrt{\pi l} \\ K_{\text{II}} = -\dfrac{2a\tau_{\text{eff}} \sin\alpha}{\sqrt{\pi(l + l^*)}}, \end{cases} \quad (14)$$

where $l^* = 0.27a$ was introduced[15] to make K_{I} and K_{II} nonsingular when $l = 0$.

At the critical condition when the wing cracks sharply begin to propagate, the wing cracks l should be 0. Accordingly K_{I} and K_{II} at the crack tips are

$$K_{\text{I}} = \frac{2a\tau_{\text{eff}} \cos\alpha}{\sqrt{\pi l^*}}, \quad K_{\text{II}} = -\frac{2a\tau_{\text{eff}} \sin\alpha}{\sqrt{\pi l^*}}. \quad (15)$$

It is known that intermittent crack does not propagate when the wing crack length $l = 0$, and accordingly, the rock mass damage remains the same. The initial damage of the rock mass induced by the original intermittent crack can be solved from eq. (10) if the stress intensity factor at the crack tip at this moment is solved. The damage from the proposed method considers both the internal factors such as rock mass and crack parameter and the external ones such as the stress condition. So the DCM for cracked rock mass obtained with the proposed method fits better with the actual condition.

If the rock mass contains multi-cracks in one row or grouped in rows, stress intensity factor at the crack tip can be calculated by the method of Li *et al.*[8].

Ashby and Hallam[19] assumed that the propagation of wing crack is mainly induced by tensile stress, and adopted K_{I} to solve the length of the wing crack. Thereafter, Huang *et al.*[15] also adopted this method to establish the corresponding DCM for a rock mass. However, studies[19] show that the wing crack propagation is not only of type I, and is often accompanied with type II, which is a mixed propagation. Therefore, the effective strain energy density criterion[19] was adopted to calculate the wing crack length. It was assumed that crack begins to propagate when the effective strain energy density (ESED) at wing crack tip is larger than the minimum strain energy density S_c.

The ESED at wing crack tip is[20]

$$S = a_{11}K_{\text{I}}^2 + 2a_{12}K_{\text{I}}K_{\text{II}} + a_{22}K_{\text{II}}^2, \quad (16)$$

where

$$a_{11} = \frac{1+\nu}{8\pi E}[(3-4\nu-\cos\theta_3)(1+\cos\theta_3)],$$

$$a_{12} = \frac{1+\nu}{8\pi E}(2\sin\theta_3)[\cos\theta_3-(1-2\nu)],$$

$$a_{22} = \frac{1+\nu}{8\pi E}[4(1-\cos\theta_3)(1-\nu)+(1+\cos\theta_3)(3\cos\theta_3-1)],$$

where θ_3 is the polar angle near the wing crack tip.

When $\theta_3 = 0$, S is the ESED at the extended direction of wing crack

$$S = \frac{1+\nu}{2\pi E}[(1-2\nu)K_{\mathrm{I}}^2 + K_{\mathrm{II}}^2]. \quad (17)$$

S_c can be expressed as[20]

$$S_c = \frac{(1+\nu)(1-2\nu)}{2\pi E}K_{\mathrm{Ic}}^2. \quad (18)$$

where K_{Ic} is the rock mass fracture toughness.

If $S \le S_c$, the intermittent crack does not propagate. When the rock mass was subjected to complex stress, eqs (11)–(13), (15) and (16)–(18) were first adopted to determine if the crack would propagate. If it does not propagate, the method proposed before can be adopted to calculate the rock mass damage under complex stress. But, if the crack propagates, the proposed method cannot be adopted to calculate the rock mass damage.

Take the model in Figure 2 as an example. Assume its dimension is 10 cm in height and 5 cm in width, and it is solved according to the planar stress problem. The parameters of crack and intact rock are shown in Table 2.

Assume the stress condition of the model is: σ_x = 5 MPa, σ_y = 20 MPa and σ_{xy} = 5 MPa. Then its damage induced by the intermittent crack along the loading direction can be obtained with the proposed model by Matlab software. According to damage theory proposed by Lemaitre[14], the damage of the cracked rock mass can be expressed as

$$E_j = (1-D)E_r, \quad (19)$$

where E_r and E_j are the Young's elastic moduli of the intact rock and cracked rock mass.

Figure 3 shows the damage and Young's elastic modulus of the cracked rock mass versus the crack dip angle for the calculation model in Figure 2. It was found that the rock mass damage begins to occur when the crack dip angle is about 21°. Then with an increase in the angle, rock mass damage increases rapidly. It has the largest damage of 0.027 when the crack dip angle is about 38°. After that, as the crack dip angle continues to increase, the crack begins to propagate and the rock mass damage begins to develop. But because only the calculation of the rock mass initial damage was studied, the rock mass damage evolution is not discussed here. Meanwhile, it was found that rock mass modulus gradually decreases with increasing damage.

The influence of other factors on rock mass damage is discussed for the proposed method. Assume the rock mass parameters adopted here are the same as above, and when the influence of one parameter on the rock mass damage is studied, the other ones are assumed to be constant. For simplicity, only the rock mass damage along the vertical direction is discussed.

Assume the crack dip angle is 35° and other parameters are as shown in Table 2, the rock mass damage versus the crack length is shown in Figure 4. It was found that the rock mass damage increases with increasing crack length, which in turn influences rock mass damage when it increases to some degree.

Assume the crack dip angle is 35° and the other parameters are as shown in Table 2, the rock mass damage versus the crack internal friction angle is shown in Figure 5. It was found that the rock mass damage decreases linearly with increasing crack internal friction angle. This is because the relationship between crack shear strength obeys Mohr-Coulomb criterion, therefore the crack shear strength will increase with increasing crack internal friction angle. Correspondingly the sample's peak strength increases and its damage decreases.

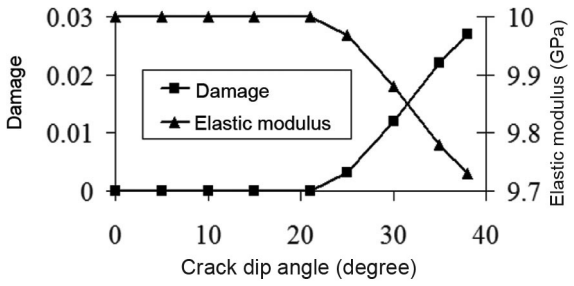

Figure 3. Variation of the rock mass damage and elastic modulus with the crack dip angle.

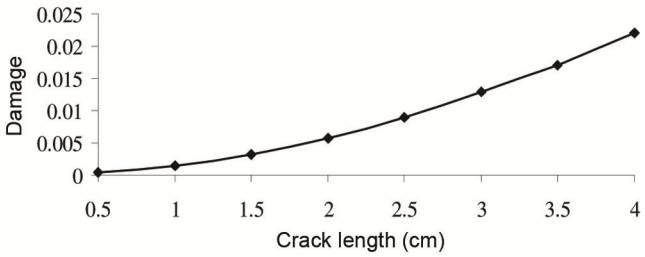

Figure 4. Variation of the rock mass damage with the crack length.

Table 2. Parameters of crack and intact rock

Crack							Intact rock	
$2a$ (cm)	B (cm)	φ/ (°)	c (kPa)	k_n (GPa/cm)	k_s (GPa/cm)	K_{IC} (MPa cm$^{1/2}$)	E (GPa)	ν
4	1	30	0.1	0.01	0.02	10	10	0.25

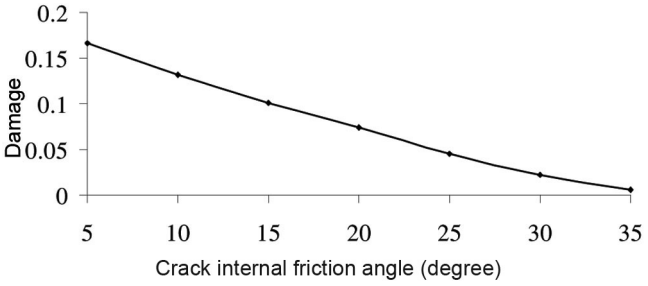

Figure 5. Variation of the rock mass damage with the crack internal friction angle.

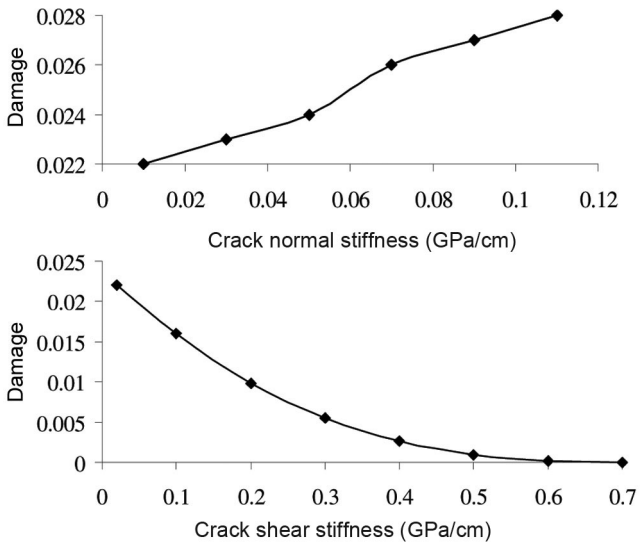

Figure 6. Variation of the rock mass damage with the crack normal and shear stiffness.

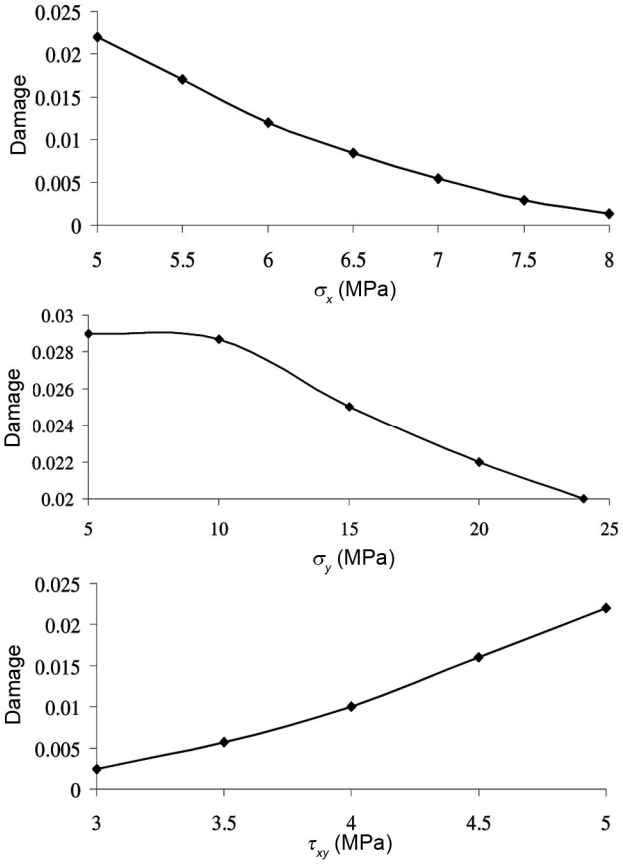

Figure 7. Variation of the rock mass damage with the stress components.

Assume the crack dip angle is 35° and other parameters are as shown in Table 2, the rock mass damage versus the crack normal and shear stiffness is shown in Figure 6. It was found that the rock mass damage increases with increasing crack normal stiffness. This is because the resolved normal stress on the crack face will decrease with increasing the crack normal stiffness from eq. (12), and therefore the friction to resist the slide of the rock block along the crack face will decrease. This will cause the rock mass to shear failure along the crack face. Therefore it leads to increase in damage and reduction in rock mass elastic modulus and strength. However, the influence of crack shear stiffness on rock mass damage is opposite that of crack normal stiffness. This is because the crack shear transferring coefficient will increase with increasing crack shear stiffness, and accordingly the shear force will decrease (see eq. (13)). Therefore, the intermittent crack will be more difficult to propagate and accordingly the rock mass damage will decrease and its elastic modulus and strength increases.

Assume the crack dip angle is 35° and other parameters are shown in Table 2, the rock mass damage versus the three stress components σ_x, σ_y and τ_{xy} is shown in Figure 7. Here it is assumed that the other two stress components remain constant when one of them changes. It was found the rock mass damage decreases linearly with increasing σ_x and σ_y, but their extent of decrease is different. With increasing σ_x, rock mass decreases linearly. While rock mass damage decreases very little when σ_y increases from 5 MPa to 10 MPa, it decreases linearly when σ_y

increases from 10 to 24 MPa. This is because with increasing vertical stress component, the crack will be compressed activating its shear strength. Meanwhile, the premise of the proposed model is that the crack in rock mass does not propagate under the external load. So, the external load is similar to the pre-stress acting on the rock mass, which makes the rock mass to be in a confined stress state. It will increase the rock mass strength and lessen its damage. However, it was also found that rock mass damage will increase with increasing τ_{xy}. This is because the rock mass is prone to shear failure under compressive and shear stress condition which leads to reduced strength and increased damage.

The existing geometry or geometry and strength damage theory for rock mass can account for the crack geometry or strength parameter, but does not consider crack deformation parameter such as its normal and shear stiffness. Meanwhile, existing studies show that rock mass damage is related not only to the crack parameter but also to loading condition of the rock mass. So, based on the connection of the increment of additional strain energy, induced by existence of crack in fracture mechanics and emission of damaged strain energy in damage mechanics, a new calculation method for the damage induced by intermittent crack to rock mass under the compressive and shear stress condition is proposed. This method considers the loading condition.

As a result, a new DCM for the intermittent cracked rock mass is proposed. It captures the co-influence of internal factors such as the crack and rock mass property but also external factors such as loading condition on rock mass mechanical property. The influence of crack length, internal friction angle, normal and shear stiffness, and the load on rock mass damage are discussed. Overall, the proposed model gives a new insights into the mechanical behaviour of intermittent cracked rock mass. However it should be stated that it is only suitable for rock mass with one group of cracks.

1. Wang, T. T. and Huang, T. H., A constitutive model for the deformation of a rock mass containing sets of ubiquitous joints. *Int. J. Rock Mech. Min. Sci*., 2009, **46**(3), 521–530.
2. Wang, T. T. and Huang, T. H., Anisotropic deformation of a circular tunnel excavated in a rock mass containing sets of ubiquitous joints: theory analysis and numerical modeling. *Rock Mech. Rock Eng*., 2014, **47**(2), 643–657.
3. Tokiwa, T. *et al*., Influence of a fault system on rock mass response to shaft excavation in soft sedimentary rock, Horonobe area, northern Japan. *Int. J. Rock Mech. Min. Sci*., 2011, **48**(5), 773–781.
4. Sari, M., The stochastic assessment of strength and deformability characteristics for a pyroclastic rock mass. *Int. J. Rock Mech. Min. Sci*., 2009, **46**(3), 613–626.
5. Sagong, M. *et al.*, Experimental and numerical analyses of an opening in a jointed rock mass under biaxial compression. *Int. J. Rock Mech. Min. Sci*., 2011, **48**(7), 1055–1067.
6. Khani, A., Baghbanan, A. and Hashemolhosseini, H., Numerical investigation of the effect of fracture intensity on deformability and REV of fractured rock masses. *Int. J. Rock Mech. Min. Sci*., 2013, **63**, 104–112.
7. Kawamoto, T., Ichikawa, Y. and Kyoya, T., Deformation and fracturing behavior of discontinuous rock mass and damage mechanics theory. *Int. J. Numer. Analy. Meth. Geomech.*, 1988, **12**, 1–30.
8. Li, N. et al., The mechanical properties and a fatigue-damage model for jointed rock mass subjected to dynamic cyclical loading. *Int. J. Rock Mech. Min. Sci*., 2011, **38**(7), 1071–1079.
9. Prudencio, M. and Van, S. J. M., Strength and failure modes of rock mass models with non-persistent joints. *Int. J. Rock Mech. Min. Sci*., 2007, **46**(6), 890–902.
10. Yang, S. Q. *et al.*, Experimental investigation on strength and failure behavior of pre-cracked marble under conventional triaxial compression. *Int. J. Solids Struct*., 2008, **45**, 4796–4819.
11. Xie, H. P., Rock and concrete damage mechanics. China University of Mining Sciences and Technology (in Chinese), Xuzhou, 1990.
12. Liu, H. Y. and Yuan, X. P., A compressive damage constitutive model for rock mass with a set of non-persistently closed joints under biaxial conditions. *Math. Probl. Eng*., 2015, 10.
13. Yang, S. Q., Crack coalescence behavior of brittle sandstone samples containing two coplanar fissures in the process of deformation failure. *Eng. Fract. Mech*., 2011, **78**, 3059–3081.
14. Lemaitre, J., How to use damage mechanics. *Nucl. Eng. Des*., 1984, **80**, 233–245.
15. Huang, C., Subhash, G. and Vitton, S. J., A dynamic damage growth model for uniaxial compressive response of rock aggregates. *Mech. Mater*., 2002, **34**(5), 267–277.
16. Paliwal, B. and Ramesh, K. T., An interacting micro-crack damage model for failure of brittle materials under compression. *J. Mech. Phys. Solids*, 2008, **56**(3), 896–923.
17. Liu, T. Y., Cao, P. and Lin, H., Damage and fracture evolution of hydraulic fracturing in compression-shear rock cracks. *Theor. Appl. Fract. Mech*., 2014, **74**, 55–63.
18. Lee, S. and Ravichandran, G., Crack initiation in brittle solids under multiaxial compression. *Eng. Fract. Mech*., 2003, **70**(13), 1645–1658.
19. Ashby, M. F. and Hallam, S. D., The failure of brittle solids containing small cracks under compressive stress states. *Acta. Metall*., 1986, **34**(3), 497–510.
20. Sih, G. C., Strain-energy-density factor applied to mixed mode crack problems. *Int. J. Fract*., 1974, **10**(3), 305–321.

ACKNOWLEDGEMENT. This study is supported by China Natural Science Funds (41162009).

Received 14 November 2016; revised accepted 8 May 2018

doi: 10.18520/cs/v115/i3/559-565